Energy and Buildings 145 (2017) 238–250

Contents lists available at ScienceDirect

Energy and Buildings

journal homepage: www.elsevier.com/locate/enbuild

Simple thermal evaluation of building envelopes containing phase change materials using a modified admittance method

Alexander M. Thiele [a], Robin S. Liggett [d], Gaurav Sant [b,c], Laurent Pilon [a,*]

[a] Mechanical and Aerospace Engineering Department, University of California, Los Angeles, Henry Samueli School of Engineering and Applied Science, United States
[b] Civil and Environmental Engineering Department, Laboratory for the Chemistry of Construction Materials (LC^2), University of California, Los Angeles, Henry Samueli School of Engineering and Applied Science, United States
[c] California Nanosystems Institute (CNSI), University of California, Los Angeles, Henry Samueli School of Engineering and Applied Science, United States
[d] Luskin School of Public Affairs, Department of Urban Planning, University of California, Los Angeles, Henry Samueli School of Engineering and Applied Science, United States

ARTICLE INFO

Article history:
Received 28 July 2016
Received in revised form 22 February 2017
Accepted 18 March 2017
Available online 24 March 2017

Keywords:
Admittance method
Decrement factor
Phase change materials

ABSTRACT

This paper extends the admittance method to predict the diurnal energy flux reduction E_r associated with adding microencapsulated phase change materials (PCMs) to single and multilayer building envelopes. The effects of phase change on the thermal load through composite building walls were accounted for by modifying the decrement factor f_{AM} and time lag ϕ_{AM}. The procedure was demonstrated for single and multilayer PCM-composite walls subjected to a constant indoor temperature and to (i) a sinusoidal sol-air outdoor temperature, (ii) a non-sinusoidal idealized sol-air temperature, or (iii) a sol-air temperature based on weather data for three different days in California climate zone 9 (Los Angeles, CA). In all cases, the analytical results for the daily thermal load passing through PCM-composite walls agreed very well with those predicted using detailed finite element simulations. The computational speed and simplicity of this procedure can enable straightforward evaluation of the energy benefits of PCM-composite walls via user-friendly design tools and platforms.

1. Introduction

For over a decade, it has been proposed to construct building envelopes using Portland cement concrete embedded with phase change materials (PCMs). Such embedment has been suggested to reduce the energy demand [1,2] and cost [3–6] associated with heating and cooling buildings. PCMs store and release thermal energy in the form of latent heat by reversibly changing phase between the liquid and solid states on a daily basis. As a result, the thermal energy transmitted into and out of a building through its envelope is reduced and delayed [6]. Phase change materials are often encapsulated in a polymeric shell to enhance their durability [7]. Significantly, full-scale demonstrations featuring building envelopes containing micro or macroencapsulated PCM have been shown to exhibit smaller indoor temperature oscillations and to require less energy for cooling than their PCM-free counterparts in various climates [8,9]. Numerical simulations have also demonstrated that the energy benefits of building envelopes with microencapsulated PCM depend on factors such as the amount and thermal properties of PCM [6], the design of the composite wall [10], and the ambient climate conditions [6,11].

The Chartered Institute of Building Services Engineers (CIBSE) recently highlighted the attractiveness of simple energy design software for less experienced users running on tablets or smart phones [12]. The CIBSE also noted that "*the thermal admittance method is particularly useful for those designers who are less experienced in building modeling, so that they can gain an understanding of the sensitivity of proposed designs to variations in the basic thermal properties of the construction*" [12]. Material models for building envelopes embedded with PCMs have been incorporated within widely-used simulation software including EnergyPlus [13–15], TRNSYS [16], and ESP-r [17]. However, such software was designed primarily for experienced researchers and engineers. On the other hand, PCMExpress [18] was developed to enable users with limited experience in thermal science and building modeling to evaluate the energy and economic benefits of PCM-composite materials. All of the above-mentioned software rely upon computationally intensive finite element methods when considering materials with temperature-dependent thermal properties such as PCM [13]. This

* Corresponding author at: Engineering IV, 420 Westwood Plaza, Los Angeles, CA 90095-1597, United States.
E-mail address: pilon@seas.ucla.edu (L. Pilon).

http://dx.doi.org/10.1016/j.enbuild.2017.03.046
0378-7788/

Nomenclature

A, B	parameters used in Eq. (A.3)
$c_{p,j}$	specific heat capacity of material "j" (J/(kg K))
f	decrement factor
E_r	energy flux reduction (%)
h	convective heat transfer coefficient (W/(m^2 K))
h_{sf}	latent heat of fusion (kJ/kg)
k_j	thermal conductivity of material "j" (W/(m K))
L_j	thickness of layer composed of material "j" (m)
L_T	total wall thickness (m)
m_j	mass of material "j" (kg)
$m_{i,j}$	ith element of layer j's transmission matrix (Eq. (A.7))
M_i	ith element of the overall transmission matrix (Eq. (A.5))
N	parameter used to determine f_S in Eq. (A.13)
q''	heat flux (W/m^2)
q''_s	solar radiation heat flux (W/m^2)
t	time (s or h)
T	temperature (°C)
T_∞	outdoor temperature (°C)
T_{pc}	PCM phase change temperature (°C)
T_{sa}	sol-air temperature (Eq. (2)) (°C)
$\bar{T}_{sa}$	daily-averaged sol-air temperature (°C)
$\bar{T}_p$	daily-averaged temperature at the center of a wall layer containing PCM (°C)
U	overall heat transfer coefficient (W/(m^2 K))
x_{PCM}	distance between the inner wall surface and the center of the PCM-layer (m)

Greek symbols

α_j	thermal diffusivity of material "j" (m^2/s)
α_s	outer wall surface total hemispherical solar absorptivity
ΔT_{pc}	PCM phase change temperature window (°C)
ΔT_n	amplitude of temperature oscillation at a location "n" (°C)
ϵ	outer wall surface emissivity
ϕ_i	time lag "i" where i = *AM*, *MW*, or *S* (h)
ϕ_j	volume fraction of material "j"
γ	factor used in Eq. (23)
ρ_j	density of material "j" (kg/m^3)
σ	Stefan–Boltzmann constant (W/(m^2 K^4))

Subscripts

AM	admittance method
c	core material (PCM)
c+s	core–shell microcapsule
i	initial
ins	insulation
l	liquid phase
L	inner wall surface
MW	Mackey and Wright
m	matrix material
max, *min*	maximum and minimum values
num	numerical
o	outer surface
p	PCM layer
pb	plaster board
s	solid phase, shell material
S	surface

could impede the implementation of such software using tablets and smartphones. Alternatively, the home energy efficient design (HEED) software was developed for users with limited engineering expertise. Instead of finite element methods, HEED [19] employs the admittance method [20] and the total equivalent temperature difference/time-averaging (TETD-TA) method [21] to assess the thermal load through building walls. However, the admittance and TETD-TA methods were derived for wall materials with constant thermal properties subjected to sinusoidal sol-air temperatures [22,23]. Thus, they cannot be used for PCM-composite walls in their present form.

The present study extends the admittance method to evaluate the thermal load through microencapsulated PCM-composite building walls. This novel procedure accurately accounts for the effects of phase change on the thermal load through building envelopes containing PCM that are subjected to realistic sol-air temperatures. The speed and simplicity of the method enables straightforward evaluation of the energy benefits of PCM-composite walls via user-friendly design tools and platforms. This facilitates the process of specifying, implementing, and adopting PCM-composite materials as building envelopes.

2. Background

2.1. Decrement factors and time lags

Analytical methods have been developed to relate the temperature $T_L(t)$ [24] and heat flux $q''_L(t)$ [20] at the inner surface of a building wall to a sinusoidal sol-air temperature $T_{sa}(t)$ at the exterior of the building. These methods have relied upon so-called decrement factors and their associated time lags. In fact, there is a family of decrement factors and time lags presented and used in the literature, each with its own physical interpretation. Unfortunately, the same terminology of "decrement factor" and "time lag" has often been used without further clarification. As a result, it can be challenging to discern which definition is being used. Appendix A provides a review of the different approaches and clarifies the definitions of the associated decrement factor and time lag. In brief, the decrement factor f_{MW}, proposed by Mackey and Wright [24], represents the ratio of the amplitude of temperature oscillation at the inner wall surface ΔT_L to that of the outdoor sol-air temperature ΔT_{sa}, i.e.,

$$f_{MW} = \frac{\Delta T_L}{\Delta T_{sa}} = \frac{T_{L,\max} - T_{L,\min}}{T_{sa,\max} - T_{sa,\min}} \tag{1}$$

where the subscripts *max* and *min* designate maximum and minimum daily values of the associated parameter, respectively. The sol-air temperature $T_{sa}(t)$ accounts for the thermal effects of outdoor air temperature and incident solar radiation flux on the outer surface of the building wall and is defined as [25],

$$T_{sa}(t) = T_\infty(t) + \frac{\alpha_s q''_s(t)}{h_o} \tag{2}$$

where α_s and h_o are respectively the total hemispherical solar absorptivity and convective heat transfer coefficient at the outer wall surface and $q''_s(t)$ is the solar radiation heat flux. The time lag ϕ_{MW} associated with f_{MW} represents the difference between the time (in hours) when the inner wall surface and the sol-air temperatures reached their respective maximum.

The decrement factor f_{AM} proposed by Danter [20] corresponds to the ratio of the periodic or cyclic thermal transmittance $\Delta q''_L(t)/\Delta T_{sa}(t)$ to the steady-state thermal transmittance or overall heat transfer coefficient U of a wall expressed as [26,22],

$$f_{AM} = \frac{\Delta q''_L}{U \Delta T_{sa}} = \frac{q''_{L,\max} - q''_{L,\min}}{U(T_{sa,\max} - T_{sa,\min})}. \tag{3}$$

Here $\Delta q''_L$ is the amplitude of the daily oscillation in the inner wall surface heat flux $q''_L(t)$. The associated time lag ϕ_{AM} represents the difference between the time (in hours) when the inner wall surface heat flux and the sol-air temperature reached their respective maximum.

Finally, several studies have defined the decrement factor f_S as the ratio of the amplitudes of oscillation in temperature at the inner ΔT_L and outer ΔT_o surfaces of a wall, expressed as [27–30],

$$f_S = \frac{\Delta T_L}{\Delta T_o} = \frac{T_{L,\max} - T_{L,\min}}{T_{o,\max} - T_{o,\min}}. \quad (4)$$

They defined time lag ϕ_S as the difference between the time (in hours) when the inner and outer wall surface temperatures reached their respective maximum. We will refer to these parameters as the surface decrement factor f_S and surface time lag ϕ_S.

2.2. Estimating thermal loads through building envelopes

Methods that estimate the thermal load through a building envelope include (i) the response factor, (ii) the total equivalent temperature difference/time-averaging (TETD-TA), (iii) the transfer function (TF), (iv) the cooling load temperature difference (CLTD), (v) the heat balance (HB), (vi) the radiant time series (RTS), and (vii) the admittance methods [21,23]. Both the admittance and TETD-TA methods rely upon decrement factors and time lags to estimate the thermal load through a building envelope. Rees et al. [21] provided an in-depth discussion of these methods and summarized the timeline of their development.

In brief, the admittance method was developed to predict the transient indoor air temperature of a room subjected to a sinusoidal outdoor sol-air temperature $T_{sa}(t)$ via analytical expressions [22]. It can account for heat conduction through the building envelope, solar radiative heat flux incident on the inner wall surfaces through windows, radiative exchange between indoor surfaces, and sensible heat storage by the indoor air. Marletta et al. [22] extended the admittance method to predict the transient indoor air temperature of a room subjected to non-sinusoidal weather conditions by decomposing the outdoor sol-air temperature into a series of harmonics using Fourier analysis. Then, the admittance method was applied to each harmonic.

Moreover, the total equivalent temperature difference $TETD(t)$ is defined as the difference between the constant indoor temperature T_{in} and the outdoor sol-air temperature $T_{sa}(t)$, i.e., $TETD(t) = T_{in} - T_{sa}(t)$, such that [23],

$$q''_L(t) = U \times TETD(t) = h_i[T_L(t) - T_{in}] \quad (5)$$

where h_i is the convective heat transfer coefficient at the inner wall surface. Mackey and Wright [24] related the inner wall surface temperature $T_L(t)$ to the sinusoidal sol-air temperature $T_{sa}(t)$ as,

$$T_L(t) = f_{MW}[T_{sa}(t - \phi_{MW}) - \bar{T}_{sa}] + \frac{U}{h_i}\bar{T}_{sa} + \left(1 - \frac{U}{h_i}\right) T_{in} \quad (6)$$

where $\bar{T}_{sa}$ is the daily-averaged sol-air temperature defined as,

$$\bar{T}_{sa} = \frac{1}{P}\int_0^P T_{sa}(t)\,dt \quad (7)$$

with $P = 86400$ s for the period of one day. Then, combining Eqs. (5) and (6), $TETD(t)$ can be expressed as a function of f_{MW} and ϕ_{MW},

$$TETD(t) = \frac{h_i f_{MW}}{U}[T_{sa}(t - \phi_{MW}) - \bar{T}_{sa}] + \bar{T}_{sa} - T_{in}. \quad (8)$$

Note that $TETD(t)$ can also be written in terms of f_{AM} [31]. Ruivo et al. [23] compared $TETD(t)$ predicted numerically and analytically for several multilayer wall constructions subjected to a constant indoor temperature and to a realistic (i.e., non-sinusoidal) sol-air temperature. The authors illustrated that $TETD(t)$ calculated using Eq. (8) agreed fairly well with numerical predictions for wall constructions with small thermal mass but agreed poorly for walls with large thermal mass. Finally, they decomposed the sol-air temperature $T_{sa}(t)$ into a Fourier series with four harmonics and superposed the $TETD(t)$ determined for each harmonic. Using this approach, the numerical and analytical predictions of $TETD(t)$ agreed very well for all wall constructions considered.

Overall, the TETD and admittance methods have been successfully applied to complex wall constructions subjected to realistic weather conditions [22,23]. However, previous studies were considering construction materials with constant thermal properties. The present study extends the admittance method to materials with temperature-dependent properties, specifically those embedded with microencapsulated PCM. The predictions of this modified admittance method were compared with those obtained from detailed numerical simulations based on finite element method for single and multilayer walls subjected to either sinusoidal or realistic sol-air outdoor temperatures.

3. Analysis

3.1. Schematic and model assumptions

Two wall configurations were considered, namely (i) a single-layer concrete slab of thickness $L_c = 10$ cm and (ii) a standard three-layer wall consisting of plaster board of thickness $L_{pb} = 1.6$ cm as the inner-most layer, wood wool insulation of thickness $L_{ins} = 5$ cm, and concrete wall of thickness $L_c = 15$ cm as the outer-most layer [26]. Figs. 1a and b illustrate the single and multilayer wall configurations, respectively, along with the coordinate system used in this study. The wall was subjected to convection to indoor air at constant temperature T_{in} with heat transfer coefficient h_i at the inner wall surface and to an outdoor air temperature $T_\infty(t)$ with heat transfer coefficient h_o at the outer wall surface. The wall was also subjected to a solar radiation flux $q''_s(t)$ at the outer wall surface.

To make the problem mathematically tractable, the following assumptions were made: (1) one-dimensional (1D) transient heat transfer prevailed in the direction perpendicular to the wall surface, (2) each wall material had isotropic and constant thermal properties except for the temperature-dependent effective specific heat, (3) the specific heat of the PCM was the same for the solid and liquid phases, and (4) contact resistances between wall layers were negligible.

3.2. Governing equations for numerical model

Under the above assumptions, the local wall temperature $T_j(x,t)$ within layer j at any time t and location x was governed by the 1D transient heat conduction equation given by [32],

$$\frac{1}{\alpha_j}\frac{\partial T_j}{\partial t} = \frac{\partial^2 T_j}{\partial x^2} \quad (9)$$

where $\alpha_j = k_j/(\rho c_p)_j$ is the thermal diffusivity and k_j, ρ_j, and $c_{p,j}$ are the thermal conductivity, density, and specific heat capacity of layer j, respectively. For cases when a layer j contained microencapsulated PCM, the effective thermal conductivity k_{eff} of the three-component composite was given by the Felske model expressed as [33],

$$k_{eff} = \frac{2k_m(1-\phi_c-\phi_s)\left(3+2\frac{\phi_s}{\phi_c}+\frac{\phi_s k_c}{\phi_c k_s}\right)+(1+2\phi_c+2\phi_s)\left[\left(3+\frac{\phi_s}{\phi_c}\right)k_c+2\frac{\phi_s k_s}{\phi_c}\right]}{(2+\phi_c+\phi_s)\left(3+2\frac{\phi_s}{\phi_c}+\frac{\phi_s k_c}{\phi_c k_s}\right)+(1-\phi_c-\phi_s)\left[\left(3+\frac{\phi_s}{\phi_c}\right)\frac{k_c}{k_m}+2\frac{\phi_s k_s}{\phi_c k_m}\right]} \quad (10)$$

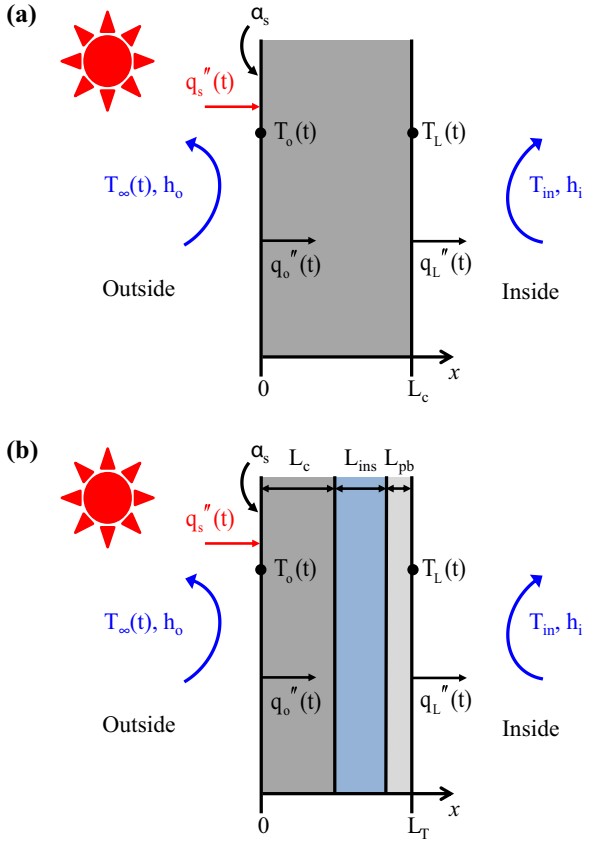

Fig. 1. Schematic of (a) a single layer wall consisting of a concrete layer of thickness L_c and (b) a multilayer wall consisting of a concrete layer of thickness L_c, an insulation layer of thickness L_{ins}, and a plaster board layer of thickness L_{pb}. Each wall was subjected to convection to a constant indoor temperature T_{in} at the inside surface ($x = L_T$) and to both convection to an outdoor air temperature $T_\infty(t)$ and solar radiation flux $q''_s(t)$ at the outside surface ($x = 0$ m). Predicting the temperatures at the inner $T_L(t)$ and outer $T_o(t)$ surfaces and the heat fluxes at the inner $q''_L(t)$ and outer $q''_o(t)$ surfaces is the focus of this study.

where k_c, k_s, and k_m are the thermal conductivities of the core, shell, and matrix, while ϕ_c and ϕ_s are the core and shell volume fractions, respectively. The Felske model has been shown to accurately account for the effects of the thermal conductivities of both core, shell, and matrix materials on the effective thermal conductivity [7]. The effective volumetric heat capacity $(\rho c_p)_{eff}(T)$ was given by [6],

$$(\rho c_p)_{eff}(T) = \phi_c(\rho c_p)_c(T) + \phi_s(\rho c_p)_s + (1 - \phi_c - \phi_s)(\rho c_p)_m \quad (11)$$

where $(\rho c_p)_c(T)$, $(\rho c_p)_s$, and $(\rho c_p)_m$ are the volumetric heat capacities of the core, shell, and matrix materials, respectively. According to the heat capacity method for simulating phase change, the specific heat capacity of the PCM core $c_{p,c}(T)$ can be defined as a step function in terms of temperature with a rectangular peak of (i) width ΔT_{pc} centered around the phase change temperature denoted by T_{pc} and (ii) enclosed area equal to the PCM latent heat of fusion h_{sf} such that [6],

$$c_{p,c}(T) = \begin{cases} c_{p,c,s} & \text{for } T < T_{pc} - \Delta T_{pc}/2, \\ c_{p,c,s} + \dfrac{h_{sf}}{\Delta T_{pc}} & \text{for } T_{pc} - \Delta T_{pc}/2 \le T \le T_{pc} + \Delta T_{pc}/2, \\ c_{p,c,l} & \text{for } T > T_{pc} + \Delta T_{pc}/2. \end{cases} \quad (12)$$

Here, $c_{p,c,s}$ and $c_{p,c,l}$ are the specific heat of solid and liquid PCM, h_{sf} is the PCM latent heat of fusion, while T_{pc} and ΔT_{pc} are the phase change temperature and temperature window, respectively.

As previously mentioned, the specific heat of solid PCM $c_{p,c,s}$ was assumed to be equivalent to that of liquid PCM $c_{p,c,l}$ (Assumption 3). The heat capacity method for simulating phase change has previously been validated against the exact solution for the one-dimensional Stefan problem [6]. We also showed that the time-dependent thermal behavior of core–shell-matrix composite materials can be accurately predicted by an equivalent homogeneous material with effective thermal properties given by Eqs. (10)–(12) [6].

3.3. Initial and boundary conditions

The initial temperature was assumed to be uniform throughout the material and equal to T_i, i.e.,

$$T(x, 0) = T_i. \quad (13)$$

In the case of a multilayer wall, the temperature and heat flux were continuous at the concrete-insulation ($x = L_c$) and insulation-plaster board ($x = L_c + L_{ins}$) interfaces (Assumption 4), i.e.,

$$-k_c \frac{\partial T_c}{\partial x}(L_c, t) = -k_{ins} \frac{\partial T_{ins}}{\partial x}(L_c, t) \quad \text{and} \quad -k_{ins} \frac{\partial T_{ins}}{\partial x}(L_c + L_{ins}, t) = -k_{pb} \frac{\partial T_{pb}}{\partial x}(L_c + L_{ins}, t). \quad (14)$$

Convective heat transfer to a constant indoor temperature T_{in} was imposed at the interior wall surface ($x = L_T$), i.e.,

$$-k_j \frac{\partial T_j}{\partial x}(L_T, t) = h_i[T_j(L_T, t) - T_{in}] \quad (15)$$

where h_i is the mixed convective heat transfer coefficient accounting for both forced and natural convections and L_T is the total wall thickness (i.e., $L_T = L_c$ or $L_c + L_{pb} + L_{ins}$). Convective heat transfer to a sol-air temperature $T_{sa}(t)$ was imposed at the exterior wall surface ($x = 0$) such that,

$$-k_j \frac{\partial T_j}{\partial x}(0, t) = h_o[T_{sa}(t) - T_j(0, t)] \quad (16)$$

where h_o is the outdoor convective heat transfer coefficient.

In a first case, the outer wall surface was subjected to a sinusoidal outdoor temperature such that $T_{sa}(t) = T_\infty(t)$, where the outdoor air temperature $T_\infty(t)$ was imposed as a sinusoidal function of time t (in s) given by,

$$T_\infty(t) = \left(\frac{T_{\infty,\max} - T_{\infty,\min}}{2}\right) \sin\left(\frac{\pi t}{43200} - \frac{2\pi}{3}\right) + \left(\frac{T_{\infty,\max} + T_{\infty,\min}}{2}\right). \quad (17)$$

Here, $T_{\infty,min}$ and $T_{\infty,max}$ are the minimum and maximum outdoor air temperatures during a day, respectively. A phase shift of $2\pi/3$ placed the peak outdoor temperature $T_{\infty,max}$ at 2:00 pm, as the daily maximum occurred between 1:00 pm and 3:00 pm for more than 80% of the year in California climate zone 9 (Los Angeles, CA), according to weather data [34]. When considering a sinusoidal outdoor temperature $T_\infty(t)$, the amplitude of temperature oscillation $(T_{\infty,max} - T_{\infty,min})/2$ was arbitrarily taken to be 7 °C and the daily-averaged outdoor temperature $\bar{T}_\infty$ was varied between 10 and 30 °C in 5 °C increments.

Second, a so-called idealized sol-air temperature was prescribed based on Eq. (2) using the sinusoidal outdoor air temperature $T_\infty(t)$ given by Eq. (17) and a solar radiation flux $q''_s(t)$ expressed as a

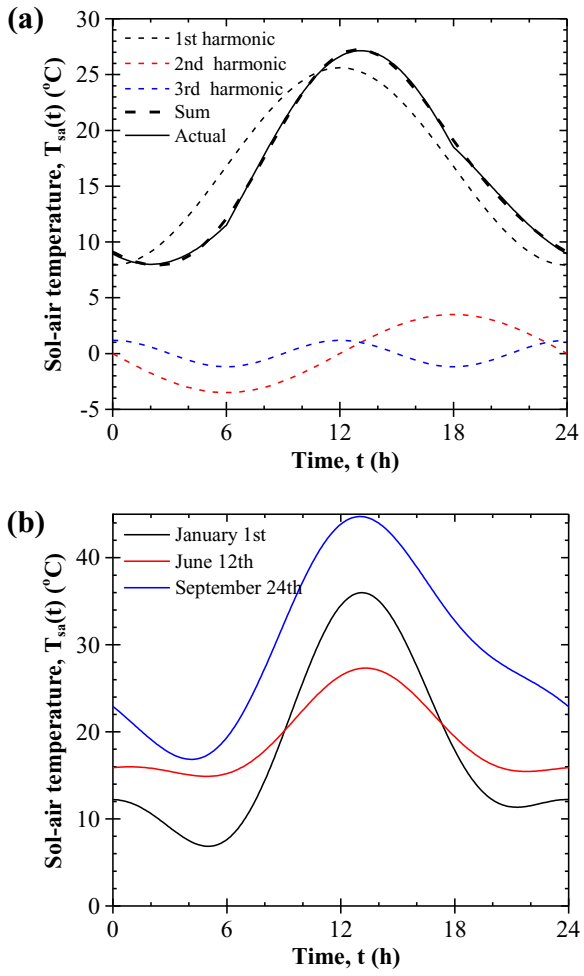

Fig. 2. (a) Idealized sol-air temperature T_{sa} as a function of time (Eqs. (2), (17), and (18)) along with its approximation as the sum of the first three harmonics of a Fourier series and (b) sol-air temperature T_{sa} as a function of time on January 1st, June 12th, and September 24th based on weather data for California climate zone 9 (Los Angeles, CA) and used as boundary conditions.

function of time t (in s) as,

$$q''_s(t) = \begin{cases} q''_{s,\max} \cos\left(\dfrac{\pi t}{43200} - \pi\right) & \text{for } 6{:}00\,\text{am} \le t \le 6{:}00\,\text{pm} \\ 0 & \text{for } 6{:}00\,\text{pm} < t < 6{:}00\,\text{am} \end{cases} \quad (18)$$

where $q''_{s,\max}$ is the maximum daily solar radiation heat flux (in W/m^2) observed at 12:00 pm and taken as 535 W/m^2, corresponding to their average value throughout the year in California climate zone 9 [34]. Fig. 2a plots the idealized sol-air temperature $T_{sa}(t)$ as a function of time given by Eq. (2) where $T_\infty(t)$ and $q''_s(t)$ were respectively defined by Eqs. (17) and (18). Here also, $(T_{\infty,max} - T_{\infty,min})/2$ was taken to be 7 °C and $\bar{T}_\infty$ was varied between 10 and 30 °C in 5 °C increments.

Finally, Fig. 2b plots the realistic sol-air temperature $T_{sa}(t)$ imposed as a function of time t based on weather data corresponding to January 1st, June 12th, and September 24th for a South-facing vertical wall in California climate zone 9 (Los Angeles, CA) [34].

3.4. Accounting for phase change in the admittance method

The decrement factors f_{MW}, f_{AM}, and f_S and their associated time lags defined in Section 2.1 are based on the assumption that the wall specific heat capacity c_p is constant. In order to account for phase change in a microencapsulated PCM-composite wall using the admittance method, we seek to define a constant modified specific heat $c'_{p,c}$ for the PCM. First, the daily-averaged temperature at the PCM-composite layer's center $\bar{T}_p$ was approximated as a linear interpolation of the daily-averaged temperatures at the inner $\bar{T}_L$ and outer $\bar{T}_o$ wall surfaces, i.e.,

$$\bar{T}_p = \frac{x_{PCM}}{L_T}\bar{T}_L + \left(1 - \frac{x_{PCM}}{L_T}\right)\bar{T}_o \quad (19)$$

where x_{PCM} is the distance from the outer wall surface at $x = 0$ m to the center of the PCM-composite layer. Such a temperature profile would prevail under steady-state conditions. According to Newton's law of cooling, $\bar{T}_L$ and $\bar{T}_o$ can be expressed in terms of the daily-averaged wall heat flux $\bar{q}''_w = U(\bar{T}_{sa} - T_{in})$ between the indoor T_{in} and the daily-averaged sol-air $\bar{T}_{sa}$ temperatures as [32],

$$\bar{T}_L = T_{in} + \frac{\bar{q}''_w}{h_i} \quad \text{and} \quad \bar{T}_o = \bar{T}_{sa} - \frac{\bar{q}''_w}{h_o}. \quad (20)$$

Similarly, the amplitude of the daily temperature oscillation at the center of the PCM-composite layer ΔT_p was approximated as a linear interpolation of the amplitudes of temperature oscillation at the inner ΔT_L and outer ΔT_o wall surfaces expressed as,

$$\Delta T_p = \frac{x_{PCM}}{L_T}\Delta T_L + \left(1 - \frac{x_{PCM}}{L_T}\right)\Delta T_o. \quad (21)$$

The amplitudes of the inner and outer wall surface temperature oscillations ΔT_L and ΔT_o can be expressed simply in terms of the decrement factors f_{MW} and f_S based on Eqs. (1) and (4).

Assuming that the temperature across the PCM-composite layer is uniform and equal to the center temperature $\bar{T}_p(t)$, the average and amplitude of temperature oscillation throughout the entire PCM-composite layer are equal to $\bar{T}_p$ and ΔT_p, respectively. Such a simplifying assumption could be justified by the fact that $\bar{T}_p$ and ΔT_p both overestimate and underestimate the values of the average and amplitude of temperature oscillation within each half of the PCM-composite layer. Then, we define the modified PCM specific heat $c'_{p,c}$ based on the energy stored in the composite wall over the temperature range $\bar{T}_p \pm \Delta T_p/2$ as,

$$[m_m c_{p,m} + m_s c_{p,s} + m_c c'_{p,c}]\,\Delta T_p = \int_{\bar{T}_p - \frac{\Delta T_p}{2}}^{\bar{T}_p + \frac{\Delta T_p}{2}} [m_m c_{p,m} + m_s c_{p,s} + m_c c_{p,c}(T)]\,dT. \quad (22)$$

Simplifying the terms appearing on both sides of Eq. (22) and substituting the expression of $c_{p,c}(T)$ given by Eq. (12) yields the following expression for $c'_{p,c}$,

$$c'_{p,c} = c_{p,c,s} + \gamma\frac{h_{sf}}{\Delta T_p} \quad (23)$$

where the coefficient γ is expressed as,

$$\gamma = \frac{\text{Min}\left(T_{pc} + \frac{\Delta T_{pc}}{2}, \bar{T}_p + \frac{\Delta T_p}{2}\right) - \text{Max}\left(T_{pc} - \frac{\Delta T_{pc}}{2}, \bar{T}_p - \frac{\Delta T_p}{2}\right)}{\Delta T_{pc}}. \quad (24)$$

Here, the coefficient γ represents the fraction of the phase change temperature window $T_{pc} \pm \Delta T_{pc}/2$ covered by the temperature oscillations at the center of the PCM composite layer $\bar{T}_p \pm \Delta T_p/2$. Note that if the phase change temperature window and range of temperature oscillations at the center of the PCM composite layer do not overlap, Eq. (24) does not apply and γ is 0.

Fig. 3 illustrates the six possible scenarios that govern the mathematical definition of γ. It plots the wall center temperature $\bar{T}_p(t)$ as a function of time for an arbitrary diurnal cycle along with the phase change temperature window ΔT_{pc}. When the range of diurnal wall temperature oscillation $\bar{T}_p \pm \Delta T_p/2$ encompasses the

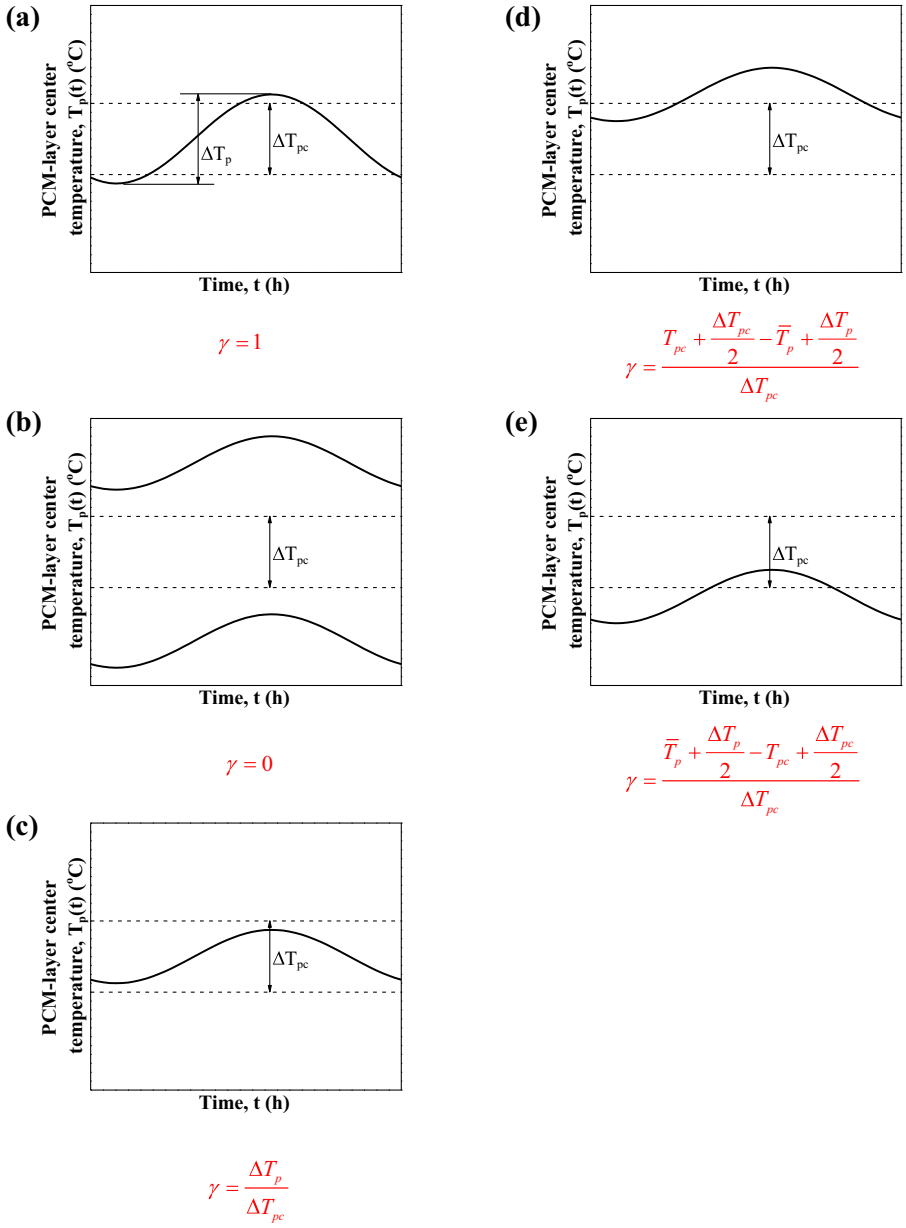

Fig. 3. Summary of the six possible scenarios of wall temperature variation relative to the phase change temperature window and the corresponding mathematical definition of γ.

entire phase change temperature range $T_{pc} \pm \Delta T_{pc}/2$, all of the PCM within the PCM-composite layer undergoes phase change and $\gamma = 1$. By contrast, if the amplitude of diurnal wall temperature oscillation $\bar{T}_p \pm \Delta T_p/2$ does not overlap with the phase change region $T_{pc} \pm \Delta T_{pc}/2$, none of the PCM within the wall undergoes phase change and $\gamma = 0$. Then, the modified PCM specific heat capacity $c'_{p,c}$ is equivalent to that of solid or liquid PCM, i.e., $c'_{p,c} = c_{p,c,s}$.

In practice, adding microencapsulated PCM to a wall has been shown to decrease the amplitude of temperature oscillation within the wall [6]. For this reason, determining the coefficient γ for a wall temperature profile without PCM would result in an overestimate. Thus, an iterative procedure was used to converge upon a value of the coefficient γ consistent with the approximated temperature oscillation within the PCM composite wall. The procedure was as follows: first, ΔT_p and γ were determined by applying the admittance method to a wall without PCM, i.e., $\phi_{c+s} = 0$. Then, the modified PCM specific heat $c'_{p,c}$ and the effective volumetric heat capacity $(\rho c_p)_{eff}$ of the PCM-composite layer with the desired microencapsulated PCM volume fraction ϕ_{c+s} were determined. The admittance method was used again with effective thermal properties to determine new values of both ΔT_p and γ. This procedure was repeated until the value of both ΔT_p and γ fell within 1% of those of the previous iteration. For all volume fractions considered, this was achieved in three iterations or less.

3.5. Constitutive relationships

Table 1 summarizes the density, thermal conductivity, and specific heat of the materials considered in this study. Wall materials included concrete [32], wood wool insulation [26], and plaster board [26]. The microencapsulated PCM consisted of the commercial organic PCM PureTemp 20 by Entropy Solution Inc. (Plymouth, MN) [35] encapsulated in high density polyethylene (HDPE) [36]. Each microcapsule was assumed to consist of 85% PCM and 15% shell material by mass [37]. Since the PCM and shell had similar densities, their volume fractions were given by $\phi_c = 0.85\phi_{c+s}$ and

Table 1
Density ρ, specific heat capacity c_p, and thermal conductivity k of PCM, high density polyethylene (HDPE), concrete, insulation, and plaster board.

Material	Subscript	ρ (kg/m^3)	c_p (J/(kg K))	k (W/(m K))	Ref.
PCM	c	860	2590	0.21	[35]
HDPE	s	930	2250	0.49	[36]
Concrete	m	2330	880	1.4	[32]
Insulation	ins	500	1000	0.1	[26]
Plaster board	pb	1320	1000	0.5	[26]

Table 2
Average sol-air temperature $\bar{T}_{sa}$ (Eq. (7)) and the coefficients a_n and b_n (Eq. (26)) that describe the Fourier series decomposition ($m = 4$) of the idealized sol-air temperature and that of California climate zone 9 (Los Angeles, CA) on January 1st, June 12th, and September 24th.

Day	$\bar{T}_{sa}$ (°C)	a_1 (°C)	b_1 (°C)	a_2 (°C)	b_2 (°C)
Idealized	$\bar{T}_\infty + 1.8$	−8.85	−3.5	1.18	0.0
January 1st	18.07	−11.14	−5.16	5.29	2.46
June 12th	19.25	−5.27	−2.13	1.91	1.44
September 24th	29.73	−10.46	−6.72	3.65	0.0

$\phi_s = 0.15\phi_{c+s}$, respectively, where $\phi_{c+s} = \phi_c + \phi_s$ is the volume fraction of microencapsulated PCM in the PCM-composite. The phase change temperature T_{pc} was taken to be equal to the indoor temperature T_{in} of 20 °C in order to maximize the reduction and delay of the thermal load through the PCM-composite wall, as suggested by recent numerical simulations [6,38]. The phase change temperature window ΔT_{pc} and the PCM latent heat of fusion h_{sf} were taken to be 8 °C and 180 kJ/kg, respectively characteristic of PureTemp 20 [35]. The indoor h_i and outdoor h_o heat transfer coefficients were respectively taken to be 7.7 and 25 W/(m^2 K), in accordance with ISO standard 6946 [39]. The total hemispherical solar absorptivity α_s of the outer wall surface was taken as 0.26, corresponding to that of white paint [32].

3.6. Data processing

As previously mentioned, the admittance method (Eqs. (A.5)–(A.9)) applies to walls exposed to sinusoidal outdoor temperature conditions. In order to determine the decrement factors f_{MW}, f_{AM}, and f_s and their associated time lags for walls exposed to non-sinusoidal conditions, the non-sinusoidal sol-air temperature $T_{sa}(t)$ was decomposed into a Fourier series with an even number m of harmonics expressed as [23],

$$T_{sa}(t) = \bar{T}_{sa} + \sum_{n=1}^{m/2} [a_n \cos(n\omega t) + b_n \sin(n\omega t)] \tag{25}$$

where the coefficients a_n and b_n are defined as,

$$a_n = \frac{2}{P}\int_0^P T_{sa}(t)\cos(n\omega t)\,\mathrm{d}t \quad \text{and} \quad b_n = \frac{2}{P}\int_0^P T_{sa}(t)\sin(n\omega t)\,\mathrm{d}t. \tag{26}$$

In the present study, the sol-air temperature $T_{sa}(t)$ was decomposed into up to $m = 4$ harmonics. For example, Fig. 2a shows three harmonics of the Fourier series decomposition of the idealized sol-air temperature $T_{sa}(t)$ given by Eqs. (2), (17), and (18). The average relative error between $T_{sa}(t)$ and its Fourier series decomposition was less than 1%.

Table 2 shows the daily-averaged sol-air temperature $\bar{T}_{sa}$ (Eq. (7)) and the coefficients a_n and b_n (Eq. (26)) of the corresponding Fourier series decomposition of the sol-air temperature (Eq. (25)) for the idealized case and for California climate zone 9 (Los Angeles, CA) on January 1st, June 12th, and September 24th. The average relative error between the actual sol-air temperature $T_{sa}(t)$ and predictions by its Fourier series decomposition was less than 6% for all three days considered. Then, the admittance method decrement factor $f_{AM,n}$ and time lag $\phi_{AM,n}$ were determined for a given composite wall configuration subjected to the nth sol-air temperature harmonic using Eqs. (A.5)–(A.9) (Appendix A) and the methodology described in Section 3.4. The corresponding inner wall surface heat flux $q''_L(t)$ was also determined by superposition according to,

$$\frac{q''_L(t)}{U} = \bar{T}_{sa} - T_{in} + \sum_{n=1}^{m/2}\left[f_{AM,2n-1}a_n \cos\left(\frac{2n\pi}{P}(t-\phi_{AM,2n-1})\right) + f_{AM,2n}b_n \sin\left(\frac{2n\pi}{P}(t-\phi_{AM,2n})\right)\right] \tag{27}$$

where $f_{AM,m}$ and $\phi_{AM,m}$ respectively represent the decrement factor and time lag corresponding to the harmonic m.

Alternatively, the decrement factor f_{AM} and time lag ϕ_{AM} for a given wall configuration were determined directly from the numerical predictions of the local wall temperature $T(x, t)$ obtained by solving Eqs. (9)–(16). Then, the conductive heat flux at the inner wall surface $q''_L(t)$ was determined based on Fourier's law, i.e.,

$$q''_L(t) = -k_j \frac{\partial T_j}{\partial x}(L_T, t). \tag{28}$$

Finally, the diurnal energy flux reduction E_r was defined as the relative difference between the daily energy fluxes (in J/m^2) through the wall without $Q''_{L,m}$ and with Q''_L microencapsulated PCM expressed as,

$$E_r = \frac{Q''_{L,m} - Q''_L}{Q''_{L,m}} \tag{29}$$

where the daily energy fluxes $Q''_{L,m}$ and Q''_L were respectively expressed as,

$$Q''_{L,m} = \int_0^{24\ h} |q''_{L,m}(t)|\,\mathrm{d}t \quad \text{and} \quad Q''_L = \int_0^{24\ h} |q''_L(t)|\,\mathrm{d}t. \tag{30}$$

The absolute values of the heat fluxes $q''_{L,m}(t)$ and $q''_L(t)$ were considered to account for the fact that there is an energy cost associated with maintaining the indoor temperature at T_{in} regardless of the direction of the heat flux across the wall. The energy flux reduction E_r describes the reduction in the daily thermal energy added or removed through a unit surface area of wall achieved by adding microencapsulated PCM.

3.7. Method of solution

The governing Eqs. (9)–(12) along with the boundary and initial conditions given by Eqs. (13)–(16) were solved using the commercial finite element solver COMSOL Multiphysics 4.4. Numerical simulations were performed for a period of up to five days and the heat flux predictions for the final day were considered. By then, the diurnal heat flux through the wall had reached a periodic steady-state and the maximum relative difference in the inner wall heat flux was less than 1% when extending the simulation period by one day. Numerical convergence was considered to be reached when the maximum relative difference in the inner wall surface heat flux $q''_L(t)$ was less than 1% when reducing the mesh size and time step by a factor of 2. In practice, converged solutions were obtained by imposing a time step of 300 s. The minimum mesh element edge size and maximum growth rate for converged solutions were 2 mm and 1.2, respectively.

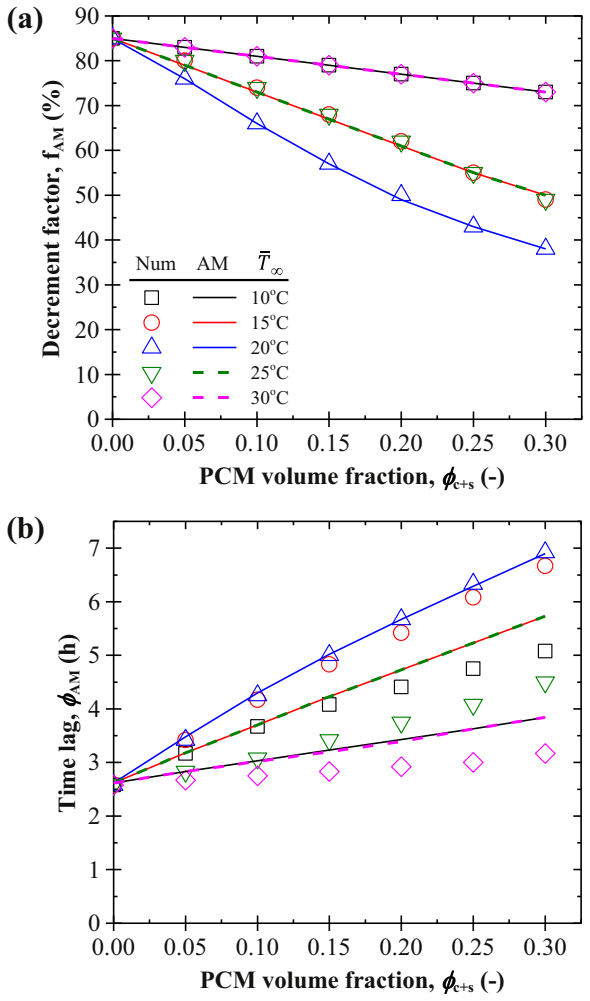

Fig. 4. (a) Admittance method decrement factor f_{AM} and (b) time lag ϕ_{AM} as functions of PCM volume fraction ϕ_{c+s} predicted numerically (Num) and using the admittance method (AM) for a composite wall subjected to a sinusoidal outdoor temperature $T_\infty(t)$ with an average value $\bar{T}_\infty$ ranging from 10 to 30 °C.

4. Results and discussion

4.1. Sinusoidal outdoor temperature

Let us first consider the case of a single-layer concrete wall containing microencapsulated PCM subjected to a sinusoidal outdoor temperature $T_{sa}(t) = T_\infty(t)$ given by Eq. (17) with amplitude of 14 °C and a daily-averaged value $\bar{T}_\infty$ ranging from 10 to 30 °C in 5 °C increments. Figs. 4a and b plot the decrement factor f_{AM} and the time lag ϕ_{AM}, respectively, as functions of microencapsulated PCM volume fraction ϕ_{c+s} ranging from 0 to 0.3 predicted numerically and using the modified admittance method. Fig. 4a shows that the decrement factor f_{AM} decreased with increasing microencapsulated PCM volume fraction ϕ_{c+s} for all outdoor temperature conditions considered. Adding microencapsulated PCM had the most dramatic effect when the average outdoor temperature $\bar{T}_\infty$ was equal to the desired indoor temperature T_{in} of 20 °C. In addition, the decrement factor f_{AM} was identical between cases where the daily-averaged outdoor temperature $\bar{T}_\infty$ was 10 °C and 30 °C as well as when it was 15 °C and 25 °C. This can be attributed to the fact that the outdoor temperature $T_\infty(t)$ was a sinusoidal function of time and T_{in} was set at 20 °C so that the same fraction of PCM changed phase in both cases. Finally, the decrement factor f_{AM} predicted using the modified admittance method agreed with numerical predictions within 2% for all outdoor temperature conditions and PCM volume fractions considered.

Fig. 4b indicates that the time lag ϕ_{AM} increased with increasing microencapsulated PCM volume fraction ϕ_{c+s} for all outdoor temperature conditions. Here also, adding microencapsulated PCM had the largest effect on the predicted time lag ϕ_{AM} when the daily-averaged outdoor temperature $\bar{T}_\infty$ was equal to the indoor temperature T_{in} of 20 °C. The numerically predicted time lag ϕ_{AM} was larger when the daily-averaged outdoor temperature $\bar{T}_\infty$ was below the indoor temperature T_{in} than when it was above T_{in}. By contrast, ϕ_{AM} predicted using the modified admittance method was identical when $\bar{T}_\infty$ was 10 °C and 30 °C as well as when it was 15 °C and 25 °C. Despite this discrepancy, the time lag ϕ_{AM} predicted numerically and using the modified admittance method fell within 1 h of each other for all temperature conditions and PCM volume fractions considered.

4.2. Idealized sol-air temperature

This section considers a microencapsulated PCM-concrete composite wall subjected not only to the same set of sinusoidal outdoor temperature $T_\infty(t)$ conditions as in Section 4.1 but also to an idealized solar radiation flux $q''_s(t)$ described by Eq. (18). The resulting idealized sol-air temperature $T_{sa}(t)$ was decomposed into a Fourier series with four harmonics (Table 2), as previously discussed and illustrated in Fig. 2a, in order to assess the thermal response of the wall using the admittance method.

Figs. 5a–c plot the inner wall surface heat flux $q''_L(t)$ as a function of time predicted numerically or by using the modified admittance method for a concrete wall containing 0, 15, and 30 vol.% microencapsulated PCM for $\bar{T}_\infty$ equal to 10, 20, and 30 °C, respectively. In all cases, adding microencapsulated PCM decreased the amplitude of oscillation of the inner wall heat flux $q''_L(t)$. Here also, adding PCM had the largest effect on $q''_L(t)$ when the average outdoor temperature $\bar{T}_\infty$ was equal to the indoor temperature $T_{in} = 20$ °C. Fig. 5b indicates that $q''_L(t)$ predicted numerically and using the modified admittance method once again agreed well when the outdoor temperature $T_\infty(t)$ was centered around T_{in}. On the other hand, Figs. 5a and c show that the inner wall surface heat flux $q''_L(t)$ predicted by the modified admittance method deviated from the numerical predictions in hot and cold climates.

Moreover, Figs. 5a and c show that the addition of microencapsulated PCM shifted the peak and trough of the numerically predicted inner wall surface heat flux $q''_L(t)$ to later times when $\bar{T}_\infty$ was 10 °C and 30 °C, respectively. This can be attributed to the fact that the numerically predicted temperature within the wall fell within the phase change region $T_{pc} \pm \Delta T_{pc}$ during the second and first half of the diurnal cycle in Figs. 5a and c, respectively. By contrast, Fig. 5b shows that adding microencapsulated PCM delayed the inner wall surface heat flux $q''_L(t)$ nearly evenly throughout the entire day. This was because the temperature within the wall fell within the phase change region for most of the day. In other words, $c_{p,c}(T)$ was nearly constant, according to Eq. (12). Similarly, the modified admittance method predicted that the inner wall surface heat flux was time-shifted uniformly throughout the day for all cases. This was due to the fact that the modified specific heat of the PCM $c'_{p,c}$ was constant. Thus, the inner wall surface heat flux $q''_L(t)$ predicted using the modified admittance method agreed most closely with numerical predictions when the outdoor temperature was such that the wall temperature was within the phase change region for most of the day.

Fig. 6 plots the diurnal energy flux reduction E_r as a function of microencapsulated PCM volume fraction ϕ_{c+s} ranging from 0 to 0.3 predicted numerically and using the modified admittance method for the same set of idealized sol-air temperature conditions

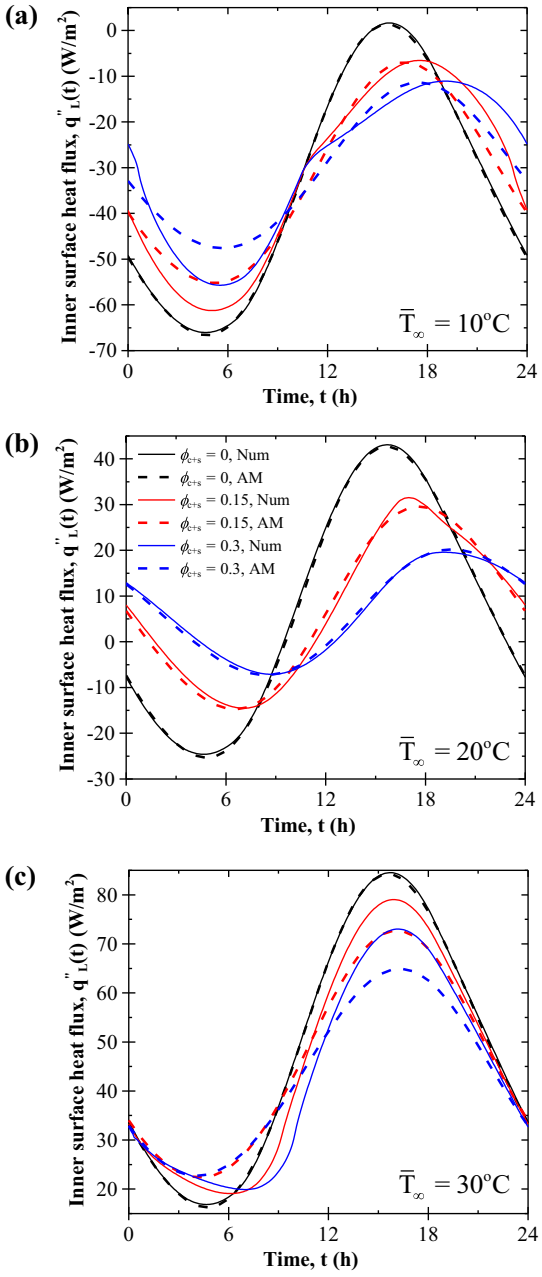

Fig. 5. Inner wall surface heat flux $q''_L(t)$ as a function of time predicted numerically (Num) and by the proposed modified admittance method (AM) for a wall containing up to 30 vol.% PCM and subjected to an idealized sol-air temperature $T_{sa}(t)$ with an average air temperature $\bar{T}_\infty$ of (a) 10 °C, (b) 20 °C, and (c) 30 °C.

considered in Fig. 5. For all cases considered, E_r increased with increasing microencapsulated PCM volume fraction ϕ_{c+s}. Here also, adding microencapsulated PCM had the largest impact on E_r when the daily-averaged outdoor temperature $\bar{T}_\infty(t)$ was equal to the indoor temperature T_{in} = 20 °C. The energy flux reduction E_r predicted using the modified admittance method agreed with numerical predictions within a relative error of 5%, despite significant disagreement in the inner wall surface heat flux $q''_L(t)$ (Fig. 5). This suggests that the energy flux reduction E_r was not significantly affected by the time lag ϕ_{AM}. Thus, the proposed modified admittance method may be used to accurately predict the diurnal energy flux reduction E_r associated with adding microencapsulated PCM to building walls subjected to idealized sol-air temperature $T_{sa}(t)$.

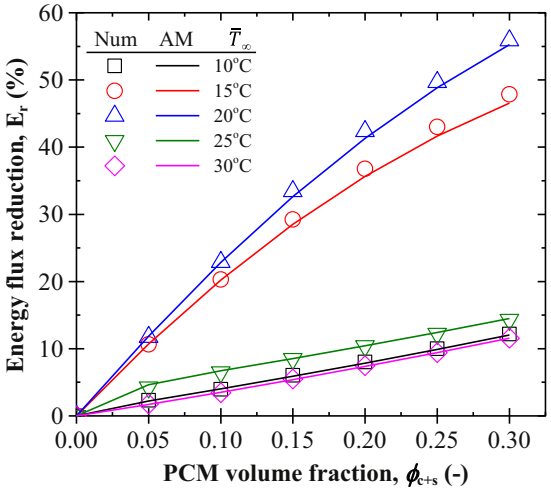

Fig. 6. Energy flux reduction E_r as a function of PCM volume fraction ϕ_{c+s} predicted numerically (Num) and using the modified admittance method (AM) for a wall subjected to an idealized sol-air temperature $T_{sa}(t)$ (Eqs. (2), (17), and (18)) with an average air temperature $\bar{T}_\infty$ ranging from 10 to 30 °C.

4.3. Realistic sol-air temperature

4.3.1. Single-layer wall

Fig. 7 plots the inner wall surface heat flux $q''_L(t)$ as a function of time predicted numerically and using the modified admittance method for a concrete wall containing 0, 15, and 30 vol.% microencapsulated PCM and subjected to a realistic sol-air temperature for (a) January 1st, (b) September 24th, and (c) June 12th, respectively. Figs. 7a and c show that the inner wall surface heat flux $q''_L(t)$ predicted numerically and using the modified admittance method agreed very well throughout most of the day for both January 1st and June 12th for all PCM volume fractions. This can be attributed to the fact that, in both cases, the sol-air temperature $T_{sa}(t)$ was centered near the phase change temperature T_{pc} = 20 °C. By contrast, Fig. 7b shows that the inner wall surface heat flux $q''_L(t)$ predicted numerically and using the admittance method agreed very poorly for September 24th when PCM was embedded in the wall, i.e., ϕ_{c+s} = 0.15 or 0.3. In these cases, the sol-air temperature $T_{sa}(t)$ only coincided with the phase change temperature window $T_{pc} \pm \Delta T_{pc}/2$ during a short period of the diurnal cycle.

Fig. 8 plots the diurnal energy flux reduction E_r as a function of microencapsulated PCM volume fraction ϕ_{c+s} ranging from 0 to 0.3 predicted numerically and using the modified admittance method for the same set of realistic sol-air temperature conditions considered in Fig. 7 and plotted in Fig. 2. The diurnal energy flux reduction E_r increased with increasing microencapsulated PCM volume fraction ϕ_{c+s}. It was slightly larger on June 12th than on January 1st. This can be attributed to the fact that the sol-air temperature $T_{sa}(t)$ had a smaller amplitude of oscillation on June 12th [6]. Predictions of E_r using the admittance method agreed within an average relative error of 6% with those based on numerical simulations. Thus, despite the complexity of actual sol-air temperature data, the proposed modified admittance method was able to accurately predict the diurnal energy flux reduction resulting from the PCM embedded in a single-layer wall.

4.3.2. Multilayer wall

Fig. 9 plots the inner wall surface heat flux $q''_L(t)$ as a function of time predicted numerically and using the modified admittance method for a multilayer wall containing 0, 15, and 30 vol.% microencapsulated PCM embedded within either (a) the concrete or (b) the plaster layer, respectively. The wall was subjected to a

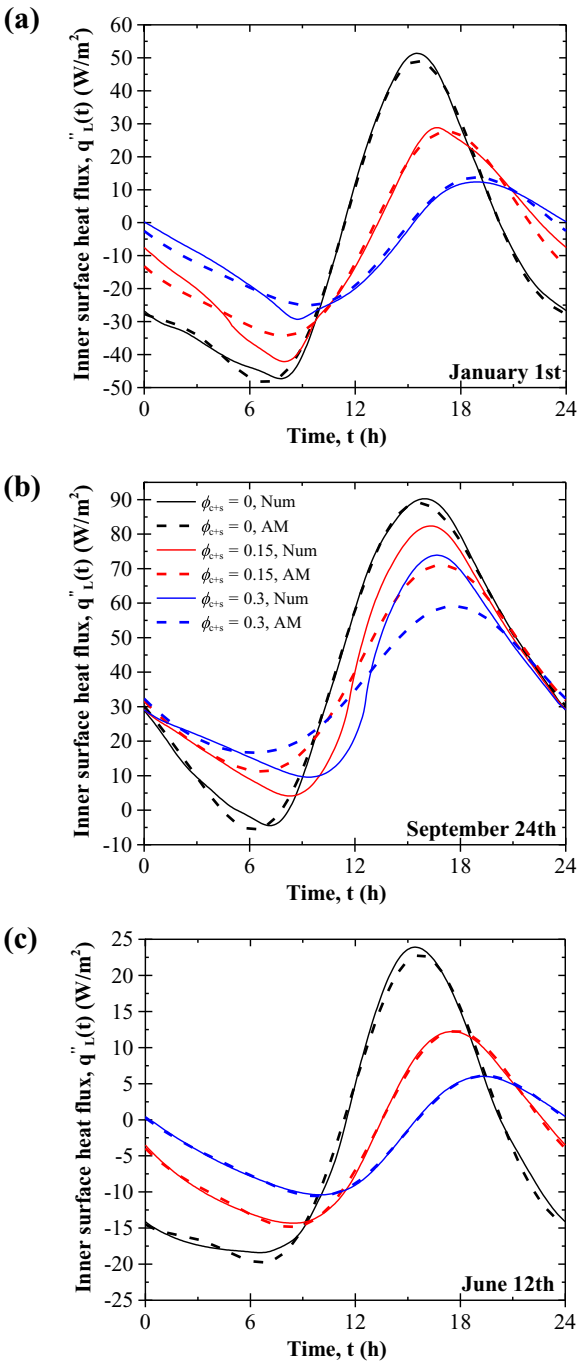

Fig. 7. Inner wall surface heat flux $q''_L(t)$ as a function of time predicted numerically (Num) and using the modified admittance method (AM) for a wall containing up to 30 vol.% PCM and subjected to a realistic sol-air temperature $T_{sa}(t)$ representative of (a) January 1st, (b) September 24th, and (c) June 12th in California climate zone 9 (Los Angeles, CA).

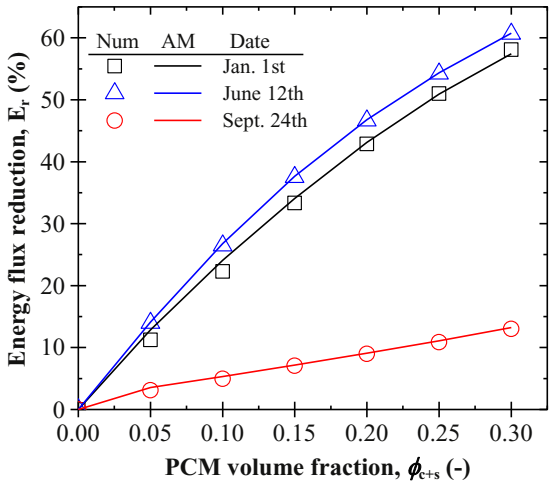

Fig. 8. Energy flux reduction E_r as a function of PCM volume fraction ϕ_{c+s} predicted numerically (Num) and using the modified admittance method (AM) for a wall subjected to a realistic sol-air temperature $T_{sa}(t)$ representative of January 1st, September 24th, and June 12th in California climate zone 9 (Los Angeles, CA).

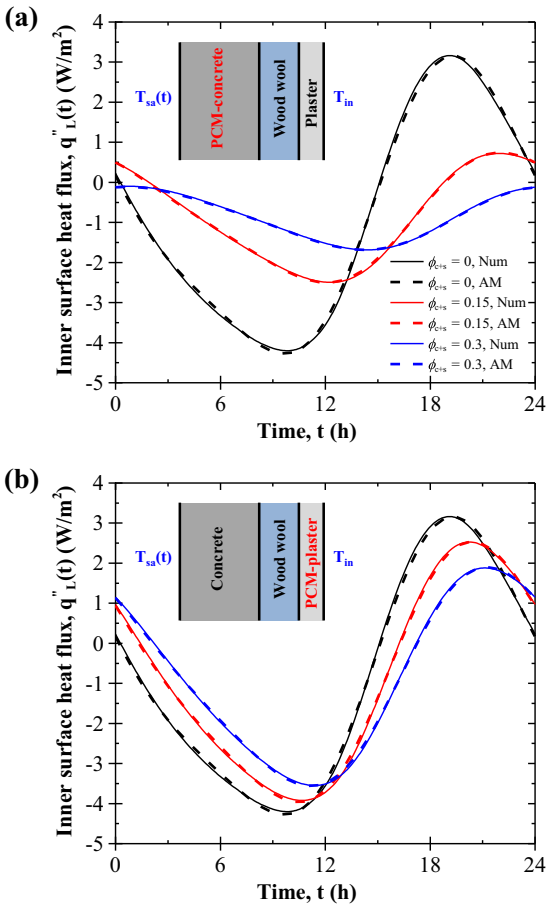

Fig. 9. Inner wall surface heat flux $q''_L(t)$ as a function of time predicted numerically (Num) and using the modified admittance method (AM) for a multilayer wall containing up to 30 vol.% PCM within (a) the concrete (outside) layer or (b) the plaster (inside) layer and subjected to a realistic sol-air temperature $T_{sa}(t)$ representative of June 12th in California climate zone 9 (Los Angeles, CA).

realistic sol-air temperature representative of June 12th. The inner wall surface heat flux $q''_L(t)$ was reduced and delayed substantially more when PCM was added to the concrete layer than to the plaster layer. This can be attributed, in part, to the fact that the PCM-concrete configuration (Fig. 9a) contained a much larger volume of PCM, for a given volume fraction ϕ_{c+s}, than the PCM-plaster configuration (Fig. 9b), due to the thicker concrete layer, i.e., $L_c > L_{pb}$. Figs. 9a and b demonstrate very close agreement between the inner wall surface heat flux $q''_L(t)$ predicted numerically and by the admittance method, regardless of which layer contained the PCM.

Fig. 10 plots the corresponding diurnal energy flux reduction E_r as a function of microencapsulated PCM volume fraction ϕ_{c+s} ranging from 0 to 0.3 predicted numerically and using the admittance method for the same multilayer wall configurations considered in

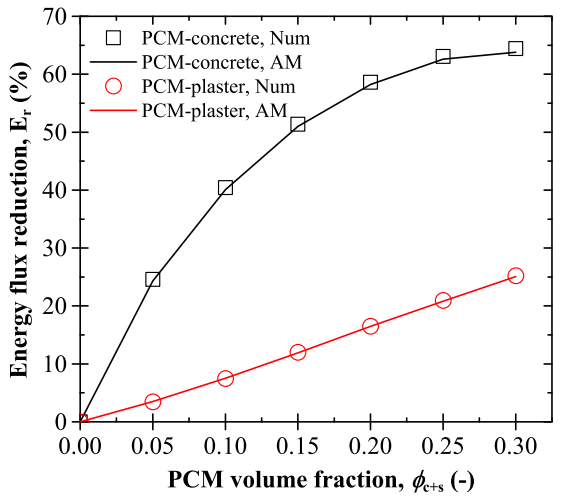

Fig. 10. Energy flux reduction E_r as a function of PCM volume fraction ϕ_{c+s} predicted numerically (Num) and using the modified admittance method (AM) for a multilayer wall containing up to 30 vol.% PCM distributed throughout the concrete (outside) layer or the plaster (inside) layer and subjected to a realistic sol-air temperature $T_{sa}(t)$ representative of June 12th in California climate zone 9 (Los Angeles, CA).

Fig. 9. It confirms that the diurnal energy flux reduction E_r was much larger when the PCM was embedded in the concrete layer than in the plaster layer, as previously discussed. The predictions of E_r using the modified admittance method agreed with those from numerical simulations within a relative error of less than 1%.

5. Conclusion

This study extended the widely-used admittance method to account for the effects of phase change on the thermal load passing through single or multilayer building envelopes subjected to realistic weather conditions. For the wide range of outdoor conditions considered, the proposed modified admittance method predicted the diurnal energy flux reduction E_r associated with adding PCM to building walls within 6% of detailed numerical predictions. However, it did not accurately predict the transient inner wall surface heat flux $q''_L(t)$ in cases where the sol-air temperature $T_{sa}(t)$ was not centered near the desired indoor temperature T_{in}. The results also obeyed previously established design rules for PCM-composite building materials, namely, (i) the diurnal energy flux reduction associated with PCM-composite walls is the largest in moderate climates with a sol-air temperature $T_{sa}(t)$ centered near the desired indoor temperature T_{in} [6,11] and (ii) the diurnal energy reduction increases as the amplitude of oscillation in the sol-air temperature $T_{sa}(t)$ decreases [6]. The speed and simplicity of the modified admittance method could facilitate the design and evaluation of the energy benefits of PCM-composite walls through user-friendly design software for a diverse group of users.

Acknowledgements

This manuscript was prepared as a result of work sponsored by the California Energy Commission (Contract: PIR:-12-032), the National Science Foundation (CMMI: 1130028) and the University of California, Los Angeles (UCLA). It does not necessarily represent the views of the Energy Commission, its employees, or the State of California. The Energy Commission, the State of California, its employees, contractors, and subcontractors make no warranty, express or implied, and assume no legal liability for the information in this document; nor does any party represent that the use of this information will not infringe upon privately owned rights. This manuscript has not been approved or disapproved by the California Energy Commission nor has the California Energy Commission passed upon the accuracy or adequacy of the information in this paper.

Appendix A. Decrement factors and time lags

Mackey and Wright [24] related the inner wall surface temperature $T_L(t)$ to a sinusoidal sol-air temperature $T_{sa}(t)$ as,

$$T_L(t) = f_{MW}[T_{sa}(t-\phi_{MW}) - \bar{T}_{sa}] + \frac{U}{h_i}\bar{T}_{sa} + \left(1 - \frac{U}{h_i}\right) T_{in} \tag{A.1}$$

where U is the overall heat transfer coefficient of the wall, $\bar{T}_{sa}$ is the time-averaged sol-air temperature, f_{MW} is the fundamental equivalent thermal resistance ratio or so-called decrement factor and ϕ_{MW} is the time lag. The decrement factor f_{MW} represented the ratio of the amplitude of temperature oscillation at the inner wall surface ΔT_L to that of the sol-air temperature ΔT_{sa}, i.e.,

$$f_{MW} = \frac{\Delta T_L}{\Delta T_{sa}} = \frac{T_{L,\max} - T_{L,\min}}{T_{sa,\max} - T_{sa,\min}}. \tag{A.2}$$

The associated time lag ϕ_{MW} represented the difference between the time (in hours) when the inner wall surface and the sol-air temperatures reached their respective maximum. The decrement factor f_{MW} and time lag ϕ_{MW} can be expressed as [24,40],

$$f_{MW} = \frac{1.414 h_o k\sigma_n}{\sqrt{A^2+B^2}} \quad \text{and} \quad \phi_{MW} = \frac{12}{\pi}\tan^{-1}\left(\frac{A-B}{A+B}\right). \tag{A.3}$$

Here, $\sigma = (\pi/86400\alpha)^{0.5}$, where $\alpha = k/(\rho c_p)$ is the thermal diffusivity and the parameters A and B were given by [24],

$$\begin{aligned} A &= (h_o + h_i)k\sigma[\cos(\sigma L)\cosh(\sigma L) + \sin(\sigma L)\sinh(\sigma L)] \\ &\quad + h_o h_i \sin(\sigma L)\cosh(\sigma L) + 2k^2\sigma^2\cos(\sigma L)\sinh(\sigma L) \\ \text{and}\quad B &= (h_o + h_i)k\sigma[\cos(\sigma L)\cosh(\sigma L) - \sin(\sigma L)\sinh(\sigma L)] \\ &\quad + h_o h_i \cos(\sigma L)\sinh(\sigma L) - 2k^2\sigma^2\sin(\sigma L)\cosh(\sigma L). \end{aligned} \tag{A.4}$$

Alternatively, Pipes [41] offered an analytical solution to the one-dimensional (1D) transient heat conduction equation for a wall subjected to convective heat transfer to a constant indoor temperature T_{in} and to a sinusoidal sol-air temperature $T_{sa}(t)$. The author related the sol-air temperature $T_{sa}(t)$ and outer wall surface heat flux $q''_o(t)$ to the indoor temperature T_{in} and inner wall surface heat flux $q''_L(t)$ as [41],

$$\begin{aligned} \begin{bmatrix} T_{sa} \\ q''_o \end{bmatrix} &= \begin{bmatrix} 1 & 1/h_o \\ 0 & 1 \end{bmatrix} \begin{bmatrix} m_1 & m_2 \\ m_3 & m_1 \end{bmatrix} \begin{bmatrix} 1 & 1/h_i \\ 0 & 1 \end{bmatrix} \begin{bmatrix} T_{in} \\ q''_L \end{bmatrix} \\ &= \begin{bmatrix} M_1 & M_2 \\ M_3 & M_4 \end{bmatrix} \begin{bmatrix} T_{in} \\ q''_L \end{bmatrix} \end{aligned} \tag{A.5}$$

where m_1, m_2, and m_3 are complex elements of the wall transmission matrix expressed as [41,22],

$$m_1 = \cosh\zeta, \quad m_2 = \frac{L}{k\zeta}\sinh\zeta, \quad \text{and} \quad m_3 = \frac{k\zeta}{L}\sinh\zeta. \tag{A.6}$$

Here, $\zeta = P + iP$, where $P = (\pi L^2/3600 t_p \alpha)^{0.5}$ and t_p is the period of the sinusoidal sol-air temperature (in hours). Note that this formulation may also be used for a multilayer wall by determining $m_{1,i}$, $m_{2,i}$, and $m_{3,i}$ for each plain-parallel layer i of the wall as a function of its thickness L_i, thermal conductivity k_i, and thermal diffusivity α_i. In other words, for a wall with n layers, Eq. (A.5) becomes,

$$\begin{bmatrix} T_{sa} \\ q''_o \end{bmatrix} = \begin{bmatrix} 1 & 1/h_o \\ 0 & 1 \end{bmatrix} \begin{bmatrix} m_{1,1} & m_{2,1} \\ m_{3,1} & m_{1,1} \end{bmatrix} \cdots \begin{bmatrix} m_{1,n} & m_{2,n} \\ m_{3,n} & m_{1,n} \end{bmatrix} \times \begin{bmatrix} 1 & 1/h_i \\ 0 & 1 \end{bmatrix} \begin{bmatrix} T_{in} \\ q''_L \end{bmatrix}. \quad (A.7)$$

Moreover, Danter [20] used the solution described by Pipes [41] for the case of constant indoor temperature T_{in} to define the decrement factor f_{AM} and the corresponding time lag ϕ_{AM} as,

$$f_{AM} = \left| \frac{1}{UM_2} \right| \quad \text{and} \quad \phi_{AM} = \frac{t_p}{2\pi} \tan^{-1} \left(\frac{\text{Im}(1/M_2)}{\text{Re}(1/M_2)} \right). \quad (A.8)$$

Considering the discontinuous nature of the inverse tangent function, it is useful to define the time lag ϕ_{AM} on a piecewise basis as,

$$\phi_{AM} = \begin{cases} \left| \frac{t_p}{2\pi} \tan^{-1} \left(\frac{\text{Im}(1/M_2)}{\text{Re}(1/M_2)} \right) \right| & \text{for } \text{Re}(1/M_2) > 0 \text{ and } \text{Im}(1/M_2) < 0 \\ \left| \frac{t_p}{2\pi} \left(\tan^{-1} \left(\frac{\text{Im}(1/M_2)}{\text{Re}(1/M_2)} \right) - \pi \right) \right| & \text{for } \text{Re}(1/M_2) < 0 \\ \left| \frac{t_p}{2\pi} \left(\tan^{-1} \left(\frac{\text{Im}(1/M_2)}{\text{Re}(1/M_2)} \right) - 2\pi \right) \right| & \text{for } \text{Re}(1/M_2) > 0 \text{ and } \text{Im}(1/M_2) > 0 \end{cases}. \quad (A.9)$$

Using this definition, the time lag ϕ_{AM} always ranges from 0 to 24 h.

The decrement factor f_{AM}, proposed by Danter [20], has been described as the ratio of the periodic or cyclic thermal transmittance $\Delta q''_L(t)/\Delta T_{sa}(t)$ to the steady-state thermal transmittance U of a wall and can be expressed as [26,22],

$$f_{AM} = \frac{\Delta q''_L}{U \Delta T_{sa}} = \frac{q''_{L,\max} - q''_{L,\min}}{U \left(T_{sa,\max} - T_{sa,\min} \right)} \quad (A.10)$$

where $\Delta q''_L$ and ΔT_{sa} are the amplitudes of oscillation in the inner wall surface heat flux $q''_L(t)$ and sol-air temperature $T_{sa}(t)$, respectively. Note that the amplitudes of oscillation in heat flux and temperature at the inner wall surface are related by $\Delta q''_L = h_i \Delta T_L$. Thus, the decrement factor f_{MW} defined by Mackey and Wright [24] is related to the decrement factor f_{AM} defined in the admittance method [20] as,

$$f_{MW} = \frac{U}{h_i} f_{AM}. \quad (A.11)$$

Furthermore, several studies have defined the decrement factor f_S as the ratio of the amplitudes of oscillation in temperature at the inner ΔT_L and outer ΔT_o surfaces of a wall. They also defined the time lag ϕ_S as the difference between the times $t_{L,max}$ and $t_{o,max}$ at which the inner and outer wall surfaces reached their maximum temperatures, respectively. Mathematically, they are expressed as [27–30],

$$f_S = \frac{\Delta T_L}{\Delta T_o} = \frac{T_{L,\max} - T_{L,\min}}{T_{o,\max} - T_{o,\min}} \quad \text{and} \quad \phi_s = t_{L,\max} - t_{o,\max}. \quad (A.12)$$

We will refer to these parameters as the surface decrement factor f_S and surface time lag ϕ_S. The solution described by Pipes [41] (Eqs. (A.5)–(A.9)) and used in the admittance method can be used to define the surface decrement factor f_S as,

$$f_S = \left| \frac{1}{h_i N_2} \right| \quad \text{where} \quad N_2 = M_2 - \frac{m_3}{h_i h_o} - \frac{m_1}{h_o}. \quad (A.13)$$

The corresponding surface time lag ϕ_S may then be determined by substituting N_2 for M_2 in Eqs. (A.8) and (A.9).

Finally, the decrement factor has also been described as the ratio of the amplitudes of oscillation in indoor and outdoor temperatures [42]. Unfortunately, it is not straightforward to reconcile this definition with those previously discussed, as f_{MW}, f_{AM}, and f_S were all defined for cases where the indoor temperature was assumed to be constant. In fact, Eqs. (A.5)–(A.9) cannot be used to define any decrement factor in the case of a time-dependent indoor temperature.

Ruivo et al. [31] identified that "*the decrement factors f_{AM} and f_{MW} of a particular wall are imperatively different and the following relationship holds: $f_{AM} = f_{MW} h_i/U$.*" The authors compared f_{AM} and f_{MW} for numerous composite wall designs and observed that predictions of f_{AM}/f_{MW} were not equivalent to h_i/U. This was likely due to the fact that the authors defined at least one of the decrement factors using some sort of graphical estimation. Indeed, if f_{MW} and f_{AM} are determined using Eqs. (A.3) and (A.4) and (A.5)–(A.8), respectively, the ratio f_{AM}/f_{MW} will always be equal to h_i/U. Ruivo et al. [31] also asserted that the time lags ϕ_{MW} and ϕ_{AM} were equivalent because "*the sol-air temperature and the outer surface temperature of the wall reach the maximum values at the same instant.*" Rather, the time lags ϕ_{MW} and ϕ_{AM} are equivalent because the temperature $T_L(t)$ and heat flux $q''_L(t)$ at a wall's inner surface ($x = L$) always reach their maximum values at the same instant.

References

[1] S.E. Kalnæs, B.P. Jelle, Phase change materials and products for building applications: a state-of-the-art review and future research opportunities, Energy Build. 94 (2015) 150–176.
[2] N. Zhu, Z. Ma, S. Wang, Dynamic characteristics and energy performance of buildings using phase change materials: a review, Energy Convers. Manag. 50 (12) (2009) 3169–3181.
[3] J. Kosny, N. Shukla, A. Fallahi, Cost Analysis of Simple Phase Change Material-Enhanced Building Envelopes in Southern US Climates, Fraunhofer Center for Sustainable Energy Systems, prepared for the US DOE Building Technologies Program, No. DOE/GO-102013-3692, 2013.
[4] A.L.S. Chan, Energy and environmental performance of building façades integrated with phase change material in subtropical Hong Kong, Energy Build. 43 (10) (2011) 2947–2955.
[5] M.M. Hassan, Y. Beliveau, Modeling of an integrated solar system, Build. Environ. 43 (5) (2008) 804–810.
[6] A.M. Thiele, G. Sant, L. Pilon, Diurnal thermal analysis of microencapsulated PCM-concrete composite walls, Energy Convers. Manag. 93 (2015) 215–227.
[7] A.M. Thiele, A. Kumar, G. Sant, L. Pilon, Effective thermal conductivity of three-component composites containing spherical capsules, Int. J. Heat Mass Transf. 73 (2014) 177–185.
[8] C. Castellón, A. Castell, M. Medrano, I. Martorell, L.F. Cabeza, Experimental study of PCM inclusion in different building envelopes, J. Sol. Energy Eng. 131 (4) (2009) 041006.
[9] A. Castell, I. Martorell, M. Medrano, G. Pérez, L.F. Cabeza, Experimental study of using PCM in brick constructive solutions for passive cooling, Energy Build. 42 (4) (2010) 534–540.
[10] S.D. Zwanzig, Y. Lian, E.G. Brehob, Numerical simulation of phase change material composite wallboard in a multi-layered building envelope, Energy Convers. Manag. 69 (2013) 27–40.
[11] A.M. Thiele, A. Jamet, G. Sant, L. Pilon, Annual energy analysis of concrete containing phase change materials for building envelopes, Energy Convers. Manag. 103 (2015) 374–386.
[12] T. Dwyer, Simple Thermal Analysis for Buildings, 2012 http://www.cibsejournal.com/cpd/2013-01.
[13] P.C. Tabares-Velasco, C. Christensen, M. Bianchi, Verification and validation of EnergyPlus phase change material model for opaque wall assemblies, Build. Environ. 54 (2012) 186–196.
[14] J.S. Sage-Lauck, D.J. Sailor, Evaluation of phase change materials for improving thermal comfort in a super-insulated residential building, Energy Build. 79 (2014) 32–40.
[15] F. Ascione, N. Bianco, R.F. De Masi, F. deRossi, G.P. Vanoli, Energy refurbishment of existing buildings through the use of phase change

materials: energy savings and indoor comfort in the cooling season, Appl. Energy 113 (2014) 990–1007.
[16] F. Kuznik, J. Virgone, K. Johannes, Development and validation of a new TRNSYS type for the simulation of external building walls containing PCM, Energy Build. 42 (7) (2010) 1004–1009.
[17] D. Heim, Isothermal storage of solar energy in building construction, Renew. Energy 35 (4) (2010) 788–796.
[18] B. Gatzka, G. Valentin, PCMExpress – planning and simulation programme for the use of phase change materials (PCM) in buildings: demonstrating its use in residential and office buildings in Ireland, in: Proceedings of the International Conference for Sustainable Energy Storage, Belfast, UK, February 21–24, University of Ulster, 2011, pp. 1–10.
[19] M. Milne, A design tool for meeting the 2030 challenge: measuring CO_2, passive performance, and site use intensity, in: Proceedings of the Solar Conference, American Solar Energy Society, American Institute of Architects, 2007.
[20] E. Danter, Periodic heat flow characteristics of simple walls and roofs, J. Inst. Heat. Vent. Eng. 28 (1960) 136–146.
[21] S.J. Rees, J.D. Spitler, M.G. Davies, P. Haves, Qualitative comparison of North American and UK cooling load calculation methods, HVAC&R Res. 6 (1) (2000) 75–99.
[22] L. Marletta, G. Evola, M. Giuga, Using the dynamic thermal properties to assess the internal temperature swings in free running buildings. A general model and its validation according to ISO 13792, Energy Build. 87 (2015) 57–65.
[23] C.R. Ruivo, D.C. Vaz, Prediction of the heat gain of external walls: an innovative approach for full-featured excitations based on the simplified method of Mackey-and-Wright, Appl. Energy 155 (2015) 378–392.
[24] C.O. Mackey, L.T. Wright Jr., Summer comfort factors as influenced by the thermal properties of building materials, Am. Soc. Heat. Vent. Eng. Trans. 49 (1943) 148–174.
[25] G. Parmelee, W. Aubele, Radiant energy transmission of the atmosphere, ASHVE Trans. 58 (1952) 85.
[26] N.O. Milbank, J. Harrington Lynn, Thermal response and the admittance procedure, Build. Serv. Eng. 42 (1974) 38–51.
[27] H. Asan, Effects of wall's insulation thickness and position on time lag and decrement factor, Energy Build. 28 (3) (1998) 299–305.
[28] H. Asan, Investigation of wall's optimum insulation position from maximum time lag and minimum decrement factor point of view, Energy Build. 32 (2) (2000) 197–203.
[29] K. Ulgen, Experimental and theoretical investigation of effects of walls thermophysical properties on time lag and decrement factor, Energy Build. 34 (3) (2002) 273–278.
[30] K.J. Kontoleon, E.A. Eumorfopoulou, The influence of wall orientation and exterior surface solar absorptivity on time lag and decrement factor in the greek region, Renew. Energy 33 (7) (2008) 1652–1664.
[31] C.R. Ruivo, P.M. Ferreira, D.C. Vaz, On the error of calculation of heat gains through walls by methods using constant decrement factor and time lag values, Energy Build. 60 (2013) 252–261.
[32] T.L. Bergman, A.S. Lavine, F.P. Incropera, D.P. DeWitt, Fundamentals of Heat and Mass Transfer, 7th ed., John Wiley & Sons, New York City, NY, 2011.
[33] J.D. Felske, Effective thermal conductivity of composite spheres in a continuous medium with contact resistance, Int. J. Heat Mass Transf. 47 (14) (2004) 3453–3461.
[34] UCLA Energy Design Tools Group, Climate Consultant, 2016 http://www.energy-design-tools.aud.ucla.edu.
[35] PureTemp 20 Technical Information, Tech. Rep., Entropy Solutions Inc., Minneapolis, MN, 2011.
[36] Typical Engineering Properties of High Density Polyethylene, Tech. Rep., INEOS Olefins & Polymers, USA, League City, TX, 2009.
[37] MPCM Technical Information, Tech. Rep., Microtek Laboratories Inc., Dayton, OH.
[38] F. Mathieu-Potvin, L. Gosselin, Thermal shielding of multilayer walls with phase change materials under different transient boundary conditions, Int. J. Therm. Sci. 48 (9) (2009) 1707–1717.
[39] International Organization for Standardization, ISO Standard 6946: Building Components and Building Elements: Thermal Resistance and Thermal Transmittance – Calculation Method, 2007.
[40] C.O. Mackey, L.T. Wright Jr., Periodic heat flow – homogeneous walls or roofs, Am. Soc. Heat. Vent. Eng. Trans. 50 (1944) 293–312.
[41] L.A. Pipes, Matrix analysis of heat transfer problems, J. Frankl. Inst. 263 (3) (1957) 195–206.
[42] F. Kuznik, J. Virgone, Experimental assessment of a phase change material for wall building use, Appl. Energy 86 (10) (2009) 2038–2046.